Matter and Radiation at Extremes | RESEARCH ARTICLE | scitation.org/journal/mre

On the design of magnetically insulated transmission lines for *z*-pinch loads

Cite as: Matter Radiat. Extremes 4, 027402 (2019); doi: 10.1063/1.5089765
Submitted: 13 September 2018 • Accepted: 12 December 2018 •
Published Online: 11 March 2019

R. B. Spielman[a] and D. B. Reisman

AFFILIATIONS

Laboratory for Laser Energetics, University of Rochester, Rochester, New York 14623-1299, USA

[a]Author to whom correspondence should be addressed: rbspielman@me.com

ABSTRACT

Many papers have been published on the theory of magnetic insulation and the use of Z_{flow} analysis of magnetically insulated transmission lines (MITLs). We describe herein a novel design process using the circuit code SCREAMER for a real-world MITL for *z*-pinch loads based on the Z_{flow} model of magnetic insulation. In particular, we design a 15-TW, 10-MA, 100-ns double-disk transmission line using only circuit modeling tools and Z_{flow} analysis of the MITL. Critical issues such as current loss to the anode during the setup of magnetic insulation and the transition from a non-emitting vacuum power feed to an MITL play a large role in the MITL design. This very rapid design process allows us for the first time to explore innovative MITL designs such as variable-impedance MITLs that provide a significantly lower total inductance and improved energy delivery to the load. The tedious process of modeling the final MITL design with highly resolved 2D and 3D electromagnetic particle-in-cell codes occurs as a validation step, not as part of the design process.

I. INTRODUCTION

The designers of magnetically insulated transmission lines (MITLs) have traditionally used analytic approaches and simple, experimentally validated design concepts as the basis for new MITL designs. Indeed, the MITLs on the original Z machine at Sandia National Laboratories[1–4] were designed using MITLs scaled from the earlier, successful Saturn MITL[5,6] and using particle-in-cell (PIC) codes primarily as the final validation process.[7–10]

Herein we describe an MITL design process that is more theoretically based than that used in earlier MITL designs. This MITL design process is supported by extensive theoretical and computational work on magnetic insulation by Creedon,[11,12] Mendel *et al.*,[13,14,18,19,21–27] VanDevender *et al.*,[15–17] Di Capua,[20] and Ottinger *et al.*[29,31,32] While this early work gave an excellent detailed theoretical description of magnetic insulation and MITL power flow, the application of MITL theory to actual MITL designs was lacking. Herein, the pulsed-power driver, the MITL, and the *z*-pinch load are modeled with the SCREAMER circuit code.[33,34] SCREAMER contains an MITL loss current model that calculates the electron current lost to the adjacent anode for each MITL segment. We can then analyze the SCREAMER output to obtain the electrical characteristics of the MITL at many points along the MITL and determine the MITL performance.

The key advantage of this MITL design approach is that design iterations are very fast, with typical circuit simulations taking ~1 min on modern computers. However, it is also important to note that this approach gives physical insight into MITL design that might not be as readily apparent if the MITL design were based solely on PIC simulations.

MITL designs should have the lowest-overall-inductance MITL that has a smooth transition region between non-emissive and emissive transmission lines; they should be consistent with the thresholds for anode plasma formation resulting from electron losses; and they should have a geometry that has smooth transitions in flow impedance (vacuum impedance, gap, etc.). While we present an MITL design for a specific driver and a specific load, the approach presented herein can be readily adapted to any driver and any load.

II. ELECTRICAL SPECIFICATIONS OF THE 15-TW DRIVER

We analyzed the MITL design for the 15-TW driver described by Spielman *et al.*[38] In this design, electrical energy from

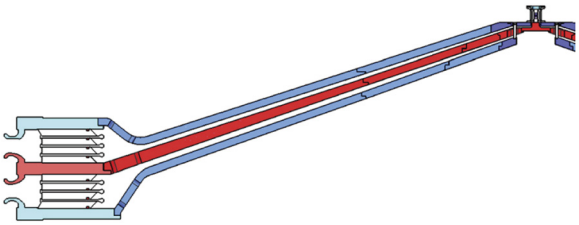

FIG. 1. (a) Schematic of the full double-disk MITL that shows the insulator stack, the vacuum flare region, the MITLs, the post-hole convolute, the inner disk MITL, and the load region. (b) Schematic showing the dimensions of the two MITLs being modeled. The 1.5-Ω impedance value is only for the radius and gap at that point. The vertical scale is expanded four times for clarity.

ten linear-transformer-driver (LTD) modules is delivered to a monolithic insulator that is composed of two separate insulator stacks. Each insulator stack is fed by one-half of the tri-plate-disk water transmission line. As shown in Fig. 1(a), each insulator stack feeds a disk MITL. In this paper, we label the disk level closest to the load [not passing through the post-hole convolute (PHC)] the A level. The lower level is the B level. The load that was modeled is a wire-array *z*-pinch. For these calculations, we used a *z*-pinch having an initial radius of 2 cm and a length of 2 cm. This has been a reference load for the Sandia Z machine since 1996.

The water transmission lines of the proposed driver can deliver a peak power up to 15 TW. The modeling described herein used the driver operating with a peak voltage of 1.25 MV in the water transmission lines at an impedance of 0.125 Ω. The resulting voltage that appears at the insulator stack is ~1.6 MV. The peak current delivered to the load is ~10 MA. The rise time of the current at the insulator stack is ~100 ns. Additional electrical details can be found in Ref. 38. The MITL analysis approach presented herein can be readily adapted to any driver and any load.

III. THE Z_{flow} MITL MODEL

MITLs were first developed in the USA in the 1970s by researchers at Physics International Co.[11,12,20] and Sandia National Laboratories.[13–19] It was a revolutionary discovery that a low-impedance vacuum transmission line could reduce or eliminate electron losses by using the self-generated magnetic field of the current losses (and load currents) themselves. It should be clear here that this approach works only with driver impedances that are low enough to generate at least the minimum magnetic field needed for insulation. We do not intend to reiterate this early work, but rather intend to show the history of magnetic insulation and how our view of magnetic insulation changed with the advent of the Z_{flow} MITL concept of Mendel *et al.*[23–28] Ottinger *et al.*[31,32] extended Mendel's work and placed it clearly in context with the earlier MITL theory, as well as providing straightforward and usable mathematical tools to calculate the relevant MITL parameters.

We can analyze an MITL when it has an equilibrium vacuum flow condition (pressure balance). In this case, Mendel and Ottinger define the MITL performance parameters in terms of a Z_{flow} parameter that describes the physical extent of the electron vacuum flow into the transmission line. Essentially, Z_{flow} is the *actual* operating impedance of the MITL and will always be less than the geometric or vacuum impedance of the MITL because of the finite thickness of the electron sheath. Various approximations are made in the definition of the Z_{flow} parameters. We typically design MITLs that are well insulated (even super-insulated), so the approximations described by Ottinger are valid here.

We can now define the parameters used in the Z_{flow} MITL design process. The vacuum impedance Z_{vac} of any portion of a transmission line is its local, geometric impedance as given by

$$Z_{vac} = \frac{V}{I} = \sqrt{\frac{L}{C}}. \tag{1}$$

The running impedance Z_r of any segment of an MITL (or vacuum power feed) is simply the ratio of the local voltage to the local current, $Z_r = V/I$. If any transmission line is terminated in a matched impedance, then $Z_{vac} = Z_r$; otherwise $Z_{vac} \neq Z_r$.

The anode current I_a is the current flowing in the anode. The cathode current I_c is the current flowing in that segment of the MITL cathode. The vacuum flow current I_{vac} is the current flowing in the electron sheath in the vacuum in that segment of the MITL. (The difference between the anode current and the cathode current is the vacuum flow current.) The vacuum flow impedance Z_{flow} is the impedance of that portion of the MITL gap that contains no electron flow. In the uniform-current-density limit, Z_{flow} can be expressed as

$$Z_{flow} = \frac{V_a}{\left(I_a^2 - I_c^2\right)^{1/2}}. \tag{2}$$

The sheath impedance Z_{sh} is the difference between Z_{vac} and Z_{flow}. The sheath impedance directly provides the sheath height h_{sh} above the cathode. One interesting MITL figure of merit is the dimensionless ratio of the local electric field to the local magnetic field, E/cB. It is somewhat surprising that E/cB is related directly to the local running impedance Z_r. A little algebra for the case of no electron flow ($I_c = I_a$, $h_{sh} = 0$, $Z_{flow} = Z_{vac}$) gives

$$E/cB = Z_r/Z_{vac}. \tag{3}$$

In the case of MITL where there is electron flow that satisfies the pressure-balance approximation of Mendel and Ottinger, the electric field in the transmission line is excluded from the electron sheath. Equation (3) is then modified as follows by replacing the vacuum impedance Z_{vac} with the reduced flow impedance Z_{flow}:

$$E/cB = Z_r/Z_{flow}. \tag{4}$$

SCREAMER simulations provide V and I_a at discrete locations in the MITL. We know the local vacuum impedance Z_{vac} for all values of *r*. With this information, we can generate Z_r, Z_{flow}, h_{sh}, I_c, I_{vac}, Z_{sh}, and E/cB. We have all of the information needed to design an efficient MITL.

Ottinger *et al.*[31,32] conveniently derived the values for the minimum anode and cathode current required for magnetic

insulation at any point in an MITL and provided the minimum value for Z_{flow} for that MITL. From Mendel, Z_{flow} is fundamentally constrained to be between $Z_{vac}/2$ and Z_{vac} since MITLs with a Z_{flow} less than $Z_{vac}/2$ would never be insulated. Ottinger provided a tighter bound on the smaller value of Z_{flow} because the Ottinger insulation limit would be larger than $Z_{vac}/2$.

From Ottinger, the minimum anode current for magnetic insulation is given by

$$I_a^{MC}(V) = \frac{V/Z_0}{f_{MC}(V)\left[2f_{MC}(V)-1\right]^{1/2}}, \quad (5)$$

the minimum cathode current for magnetic insulation by

$$I_c^{MC} = \frac{2^{1/2}(1-f_{MC})^{1/2}}{f_{MC}(2f_{MC}-1)^{1/2}}\frac{V}{Z_0}, \quad (6)$$

and the minimum value for Z_{flow} by

$$Z_f^{MC}(V) = Z_0 f_{MC}(V), \quad (7)$$

where $Z_0 = Z_{vac}$ and $Z_f = Z_{flow}$. The constant f_{MC} is given by

$$f_{MC}(V) = \frac{\left(\frac{gmc^2}{8\,eV}-1\right) + \left[\left(\frac{gmc^2}{8\,eV}-1\right)^2 + \left(\frac{gmc^2}{2\,eV}-1\right)\right]^{1/2}}{\left(\frac{gmc^2}{2\,eV}-1\right)}, \quad (8)$$

where m is the electron mass, c is the speed of light, e is the electron charge, and the parameter g, $g(V) = 0.995\,65 - 0.053\,32V + 0.0037V^2$, is a scale factor that is close to 1 and is generated by running many highly resolved PIC simulations.

In addition, Ottinger gave an equation for Z_{flow} [Z_f in Eqs. (7)–(9) here] that is based only on the measured current and voltage of the MITL and Z_0 (Z_{vac}). The flow impedance is presented as a nonlinear equation where we are looking for solutions (real roots) for which the remainder error $h(Z_f)$ is zero. This equation will have three roots with at most two real roots. The input parameters are voltage V, anode current I_a, and vacuum impedance Z_0. The equation is as follows (we use Ottinger's formalism exactly here):

$$h(Z_f) = Z_f^3 - Z_0 Z_f^2 + \left(\frac{gmc^2 V}{2eI_a^2} - \frac{V^2}{I_a^2}\right)Z_f + \frac{Z_0 V^2}{I_a^2} = 0, \quad (9)$$

where m, c, e, and g are as above. Equation (9) can be solved iteratively to find the desired real roots. The real root closest to Z_0 (Z_{vac}) is the solution for the most highly insulated root. There are rare cases when one is close to the minimum anode current where there can be two solutions to the equation.

IV. MITL DESIGN CRITERIA

Calculation of the Z_{flow} parameters is a necessary but not sufficient condition to design a real-world MITL. Some of these issues were described by Stygar *et al.*,[35] Savage *et al.*,[36] and VanDevender *et al.*[37] Three key issues must be addressed in order to design a working MITL:

(1) electron losses to the anode during the setup of magnetic insulation;
(2) the transition region between non-emissive and emissive transmission lines; and
(3) transitions in MITL dimensions, shape, and impedance as a function of location.

A. Electron losses to the anode

Electrons must be lost early on during the onset of magnetic insulation. The magnitude of the loss current (density) is approximately that of Child–Langmuir space-charge-limited electron loss until B is large enough for the Larmor radius to be less than about one-half the local MITL gap h. The electron losses scale as h^{-2} and $V^{3/2}$, and larger anode–cathode (AK) gaps have smaller electron losses to the anode. Consequently, we do not have arbitrary flexibility to choose a small-gap (low-impedance) MITL, even if that MITL satisfied the Z_{flow} design criteria, since, eventually, sufficient electrons will be lost to the anode to heat the anode above the empirically determined ~400 °C threshold for desorption of hydrogen from the anode and create an anode plasma.[39] Any MITL design must consider the issue of anode heating at *all* locations in the MITL. At the same time, it adds no value to have one small portion of the MITL just safe from electron-loss current density and have the remainder of the MITL very safe with much less electron-loss current density. One could design an MITL to have the same "safe" current density loss at each segment of the MITL. This gives an MITL with a lower inductance. SCREAMER provides the electron-loss current density averaged for each MITL segment. By dividing the entire MITL into many smaller MITL segments, it is possible to get a good estimate of the MITL losses as a function of radius along the disk MITL.

B. Transition region to magnetic insulation

Any real pulsed-power vacuum feed has a transition from the permanently non-emissive region near the insulator stack to a full-fledged MITL [shown in Fig. 1(a)]. Why is this a concern? Data[1,4] have shown that abrupt transitions to an MITL result in losses that are discrete in azimuth. The data show that we want to spread out the radial extent of electron emission in the transition region of the cathode. The rule of thumb on the Z machine was that the radial transition from a no-emission vacuum feed to a full-emission MITL was ~10 cm. The quantitative reasons for this are not clear, and detailed physics understanding of these electron losses to the anode will require a highly resolved, 3D PIC simulation of that region of the MITL.

C. MITL transitions

Once magnetic insulation is established, changes to the key Z_{flow} MITL parameters radially along the MITL should be gradual. Extensive data from Sandia's Z machine showed that vacuum insulation remains very good, even though there are slow changes to the MITL Z_{vac} over ~10 cm of radius. Empirically then, we can restate this slow transition rule as: The Z_{flow} MITL parameters (Z_{flow}, I_{vac}, h_{sh}) must all have small, gradual changes over the region of transition. Simulations by Pointon *et al.*[9]

clearly show that abrupt changes in Z_{vac} will cause electron losses.

The Z_{flow} MITL parameters such as Z_{flow}, I_{vac}, h_{sh}, and E/cB depend on the local MITL impedance. Qualitatively, decreases in MITL gap (decreases in impedance) will decrease Z_{flow} and increase I_{vac}, h_{sh}, and E/cB. The designer must be cautious whenever the local Z_{flow} approaches one-half Z_{vac} and when $E/cB \sim 1.0$. In fact, there are cases with Z_{flow} higher than one-half Z_{vac} that are not well insulated.

V. A CONSTANT-IMPEDANCE MITL DESIGN FOR *z*-PINCH LOADS

The simplest approach to disk MITL design is to use a constant-impedance disk MITL until one is near the PHC. This design is shown schematically in Fig. 1(a). This is the design used on the Sandia Z machine that was originally designed in 1994–1995 and commenced operation in 1996. In that case, the A- and B-level disk MITLs had a constant impedance of ~2 Ω for most of the MITL radial extent, where the vacuum impedance Z_{vac} of a disk MITL is

$$Z_{disk} = \sqrt{\frac{\mu_0}{\varepsilon_0}}\,\frac{h}{2\pi r}, \tag{10}$$

where h is the electrode spacing and r is the radius at that point in the feed.

The simple case for an MITL of a constant vacuum impedance Z_{vac} terminated in a matched impedance is a vacuum feed having a constant voltage and constant current along the MITL. This means that $Z_r = Z_{flow}$ and Z_{flow} is constant along the MITL, and therefore E/cB is also constant in the MITL. The current in the vacuum electron flow, I_{vac}, is constant along the MITL. The electron sheath height h_{sh}, as a fraction of the MITL gap, is constant (shrinking in absolute terms).

The case of an MITL of a constant vacuum impedance Z_{vac} terminated in an impedance lower than the vacuum impedance is interesting. In this case, we have a vacuum feed with a constant voltage and constant current along the MITL, but we find that $Z_{flow} \neq Z_r$. Any termination impedance that is lower than Z_{vac} gives a Z_r that is lower than Z_{vac}. Again, Z_{flow} is constant along the MITL and, therefore, E/cB is also constant in the MITL, but in this case E/cB is *lower* than the matched case. The electron current in the vacuum electron flow I_{vac} is constant along the MITL but lower than in the matched case. The actual electron sheath h_{sh} as a fraction of the MITL gap is constant but smaller than in the matched case.

In reality, the MITLs driving a dynamic z-pinch load are essentially driving a purely reactive short-circuit load. Until peak current (~100 ns), the total circuit inductance is nearly constant. This means that the MITL is terminated in a short circuit with an effective inductance in series with the MITL. We describe such a load as very undermatched. In our case, the length of the MITL is short compared with the pulse length, so the entire MITL is load-dominated at all times. Very undermatched loads have the effect of lowering the voltage on the MITL by up to a factor of 2 and increasing the current by up to a factor of 2 over the matched case. It is easy to see that E/cB decreases by up to four times as well. This is a very good thing for magnetic insulation. Another qualitative consequence of this sort of undermatched load is that Z_r decreases radially inward and decreases in time after peak voltage and before peak current. This is translated directly to E/cB decreasing in radius and time (after peak MITL voltage).

We model idealized disk MITLs that extend from the region near the insulator stack to the constant-gap MITL section at a radius of 30 cm. The initial height of the vacuum feed at a radius of 155 cm is 11.43 cm. Figure 1(b) includes the vacuum flare at an angle of ~31.7° and shows the electrode profile for a constant 2-Ω disk MITL. The drawing provides detailed radial location and gap dimensions. Note that the vertical scale in the figure is four times the horizontal scale for clarity.

The inductance of a 2-Ω MITL with a length of 4.038 ns is 8.076 nH by inspection. The total inductance of the vacuum feed and load in these calculations is 10.56 nH. This inductance is the paralleled inductance of the A- and B-level feeds, the PHC, the disk MITL, and the load.

A. *SCREAMER* simulation of a 2-Ω MITL

We now describe the results of SCREAMER[33,34] calculations for the B-level MITL of a 15-TW pulsed-power driver. The B-level circuit includes the series inductance of the PHC, so it is the worst magnetic-insulation case (compared with the A level). (The detailed SCREAMER run deck for this case is available upon request.) We treat each disk MITL (A and B levels) totally independently, but then combine them to drive a single z-pinch load. For the purposes of this simulation, we model a z-pinch load that is 2 cm in radius and 2 cm in length. The z-pinch mass is set to ~1.5 mg so that the implosion time is ~100 ns. (This is the reference Sandia Z machine Z51 load with the mass scaled by $\sim I^2$.) The disk MITL impedances are a constant 2 Ω (the same as on the Z machine), and each disk feeds a short 1-cm constant-gap section of the MITL, the PHC, the inner MITL, and the z-pinch. (Note that the final machine design would not really be constant-impedance, since there are impedance transitions on the entrance and exit of the MITL.) For these calculations, each disk MITL is divided into ten MITL segments (each 0.4012 ns long), with each MITL segment providing V, I, and the loss current density J_{loss}. This means one can quantify the electron losses (current and current density) *in each individual MITL segment*. In SCREAMER, we use the standard MITL-loss model that has been used for more than 20 years for early-time electron losses. The simulation results are post-processed to give Z_{flow} parameters. (The Fortran code for this calculation can be provided upon request.) We know the vacuum impedance at each MITL location from the MITL geometry. With V, I, and Z_{vac}, we have enough information to derive Z_{flow}, I_c, I_{vac}, and h_{sh} at those MITL segments in time. We choose the time of peak voltage on the MITL for a detailed Z_{flow} analysis for the purposes of this paper. This is the most stressing time for the feed (maximum electric field, lowest magnetic field, and the largest E/cB).

A SCREAMER calculation for our driver using 2-Ω constant-impedance MITLs and a Z51 wire-array z-pinch load gives us detailed voltage, current, and MITL information in time. The overall current performance is shown in Fig. 2, where we plot the total current in the load and the current exiting the

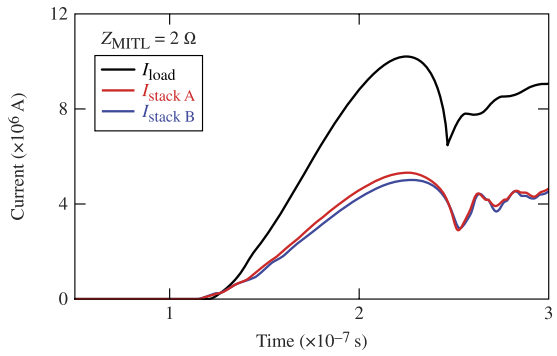

FIG. 2. Calculated total current (black solid curve), A-level current (red solid curve), and B-level current (blue solid curve) as functions of time.

A- and B-level MITLs. The A- and B-level currents reflect their differing inductances and their different electron losses to the anode in the MITLs. The total current includes additional losses in the vacuum PHC, not discussed here, that exist mainly at the time of implosion. We see that the peak current driving the load is ~10 MA. Again, it is instructive to note that the sum of the A- and B-level MITL currents *do not* add up to the load current, especially after peak current. This is because of electron losses in the PHC that increase with increasing PHC voltage at the time of implosion.

The detailed current profiles at the ten MITL locations in the B-level MITL are shown in Fig. 3. Here, the current in each MITL segment of the B level is shown individually. They are all different because of differing local MITL losses. The current at the B-level insulator stack (I_stack_B) bounds the MITL currents on the high side, and the current out of the final MITL segment bounds the current on the low side. Again, the differences in the MITL currents reflect the varying electron losses in the individual MITL segments. The MITL current information in Fig. 3 is from the ten radial locations immediately *after* each MITL segment.

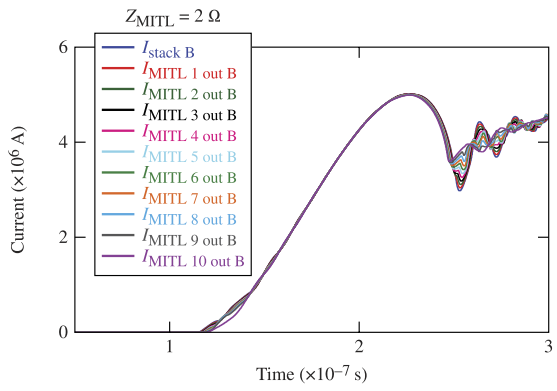

FIG. 3. Calculated currents in each MITL segment as functions of time. The differences seen in the time window from 120 ns to 140 ns reflect losses during the setup of magnetic insulation.

In Fig. 4, we plot the voltages out of each MITL segment. The voltages of each MITL segment decrease as the MITL radii decrease, owing to reduced enclosed inductance.

Table I also gives the various electrical parameters of the MITL at the time of peak MITL voltage (175 ns) for reference. The local electric field at each MITL segment is calculated and also shown in Table I. The AK gap is the gap at the center of that MITL segment with the radius given. The anode current I_a is measured at 175 ns. The cathode electric field E_c is the anode voltage at 175 ns divided by the gap at that location. We then calculated the Z_{flow} parameters for each segment of the MITL.

Several items of interest can be seen in Table I:

1. Note that the Z_r decreases strongly with decreasing radius. It will eventually approach the driving impedance of 0.25 Ω. This is caused by the reduction in local voltage with radius. This voltage drives the ratio E/cB, which decreases strongly with decreasing radius. This means that the "quality factor" for magnetic insulation is slowly increasing with decreasing radius. This is very good.
2. The flow impedance Z_{flow} increases very weakly with decreasing MITL radius. (Z_{flow} cannot be larger than Z_{vac}, so the difference between Z_{vac} and Z_{flow} is getting smaller.) This implies that the quality of magnetic insulation is slowly improving with decreasing radius.
3. The cathode current (directly from Z_{flow}) increases with decreasing radius. This means that the fraction of the current in the vacuum electron flow is decreasing with decreasing radius. Again, this means that magnetic insulation is improving with decreasing radius. The amount of current in the vacuum electron flow is trivial compared with the total B-level current.
4. The size of the electron sheath, h_{sh}, decreases with decreasing radius as driven by Z_{flow}. This is true even as a fraction of the gap. The electron sheath is remarkably thin (a fraction of a millimeter). This is very good for magnetic insulation.
5. Since these electrical parameters are taken at peak MITL voltage with a rising current, all of the magnetic-insulation Z_{flow} parameters discussed above improve later in time until peak current (voltage falls and current increases).

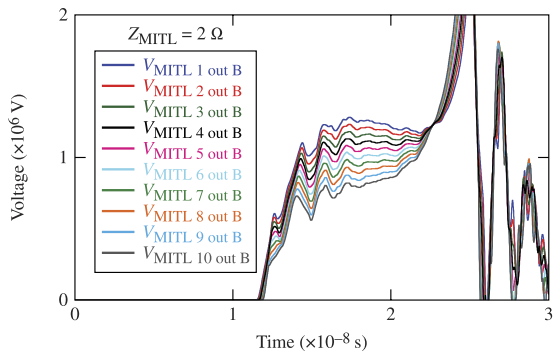

FIG. 4. Calculated voltages in each MITL segment as functions of time.

TABLE I. Listing of the MITL parameters from the ten MITL segments on the B level from *SCREAMER* calculations for a 2-Ω constant-impedance MITL.

MITL segment	Radial location (cm)	AK gap (cm)	Z_{vac} (Ω)	V_a (MV)	E_c (kV/cm)	I_a (MA)	Z_r (Ω)	Z_{flow} (Ω)	I_c (MA)	I_{vac} (kA)	E/cB	h_{sh} (mm)	h_{sh}/gap
1	144.95	4.835	2	1.28	265	2.77	0.462	1.978	2.693	77	0.234	0.52	0.0108
2	132.85	4.431	2	1.22	275	2.77	0.440	1.980	2.701	69	0.223	0.45	0.0101
3	120.75	4.028	2	1.17	290	2.77	0.422	1.980	2.706	64	0.213	0.40	0.0099
4	108.65	3.624	2	1.12	309	2.77	0.404	1.981	2.712	58	0.204	0.34	0.0094
5	96.55	3.220	2	1.07	332	2.77	0.386	1.982	2.717	53	0.195	0.29	0.0088
6	84.45	2.817	2	1.01	359	2.77	0.365	1.983	2.723	47	0.184	0.24	0.0083
7	72.35	2.413	2	0.966	382	2.77	0.349	1.984	2.727	43	0.176	0.19	0.0080
8	60.25	2.010	2	0.906	451	2.77	0.327	1.985	2.732	38	0.165	0.15	0.0075
9	48.15	1.606	2	0.855	532	2.77	0.309	1.986	2.736	34	0.155	0.11	0.0071
10	36.05	1.202	2	0.803	668	2.77	0.290	1.986	2.740	30	0.146	0.08	0.0068

6. The peak value of the electric field (at 175 ns) increases radially inward. Early in time, this means that the cathode of the innermost MITL segment (segment 10) will start emitting electrons (self-limited) before any of the other MITL segments, because its electric field will exceed the electron-emission threshold first. As the applied voltage continues to increase, after the start of electron emission from MITL segment 10, MITL segments at larger radii start to emit electrons. One can think of the emission front moving outward, *not* inward as is presented in many papers.

At peak voltage, the 2-Ω MITL is becoming more safely insulated with decreasing radius. The calculated reduction in the vacuum-electron-flow current means that electron retrapping is taking place. The fraction of the current in vacuum flow is insignificant *even at peak voltage* and, even if all of that vacuum-electron-flow current is lost at the PHC, it is not a significant current loss. [Note that the magnitude of electron losses at the PHC depends on the convolute voltage, and those losses increase dramatically with peak driver current (PHC voltage), as was seen going from Z to ZR.] These MITL behaviors are typical with *z*-pinch loads that are effectively a short circuit until peak current, after which the dL/dt voltage makes magnetic insulation more perilous. This type of MITL is referred to as a super-insulated MITL by Ottinger *et al.*[30–32] We can safely predict that there will be no losses in this 2-Ω B-level disk MITL after magnetic insulation is established.

We plot the electron-loss current to the anode in the B-level MITL segments in Fig. 5 and the loss current density in the B-level MITLs in Fig. 6. The calculations of the loss current density in each segment of the MITL show that the lowest loss current density is on the outer MITL segments (largest gap), with increasing loss current density on the inner MITL segments. The loss current is very sensitive to the MITL gap (impedance), and the relatively large electron losses seen on MITL segment 10 can be reduced significantly by only slightly increasing the MITL gap at that location.

Figure 5 shows that the electron-loss current starts at the inner MITL segments because it is in those locations that the cathode electric field first exceeds the 200-kV/cm threshold, which is the default emission threshold in SCREAMER. This is just as implied from the values of E_c in Table I. Later in time, the electron losses expand radially outward until there are losses in all MITL segments. As the B-level MITL current rises, the inner segments become insulated first because the magnetic field is higher at those locations. The last MITL segment to be fully insulated is the outer MITL segment 1.

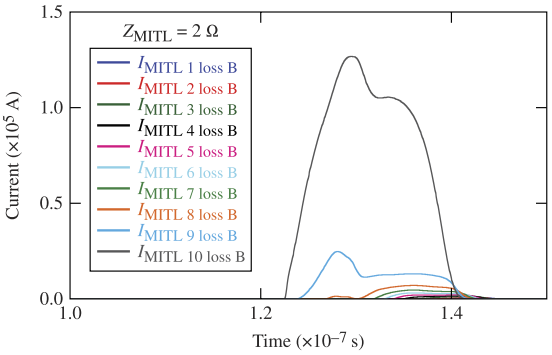

FIG. 5. Electron-loss currents in each MITL segment, where the largest current losses occur with the inner MITL segment 10. *z*-pinch stagnation is at ~255 ns.

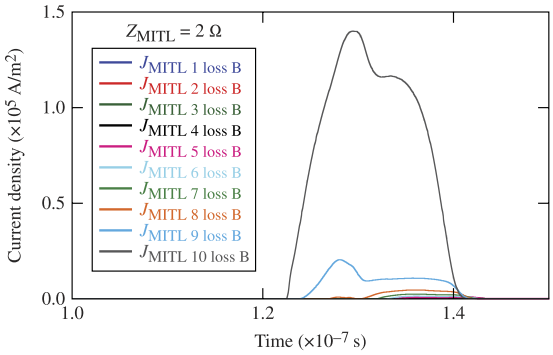

FIG. 6. Electron-loss current density in each MITL segment, where the largest current density losses occur with the inner MITL segment 10.

The electron-loss current density plot of Fig. 6 shows an attempt to normalize the losses by the area of that segment of the MITL. This tells us the relative importance of the losses in the different MITL segments. We see that the electron current density losses in the *outer* MITL segments are ~1000 times lower than those in the *inner* MITL segments.

The detailed anode deposition energy and anode temperature rise, caused by these electron losses, need quantitative results from a high-resolution PIC simulation with electron-energy deposition in the anode and anode heating (ITS Tiger post processor[40]). For our simulations, we simply assume that the electron energy for all of the losses is the same and that the deposition in the anode is the same. Thus, we simply choose a maximum-allowed current density (actually areal charge lost) for the MITL segments based on data from previous experiments. Since the outer MITL segments see less electron-loss current density (and lower integrated charge lost) than the inner MITL segments, we can safely assume that decreased MITL gaps at those outer locations (to increase the local losses) are permitted.

We conclude that a 2-Ω constant-impedance MITL will have minimal electron losses during the setup of magnetic insulation in the outer disk MITL and measurable losses in the inner disk MITL (still lower than the losses on the working Sandia Z-machine MITLs). The quality of the magnetic insulation at peak MITL voltage is very good, and the magnetic insulation quality is increasing with decreasing radius and increasing time. This 2-Ω vacuum feed is a very safe, first-cut MITL design—just as the vacuum feed was on the Z machine. The MITL design will work well for the 15-TW driver that we are modeling. Again, the fact that the electron-loss current density is *much* lower at larger radii than at smaller radii suggests that improvements in the MITL design, lowering inductance, can be made.

VI. A VARIABLE-IMPEDANCE MITL DESIGN FOR *z*-PINCH LOADS

What can we do to improve the coupling efficiency of the driver to the load? The energy-coupling efficiency to a z-pinch load improves with decreasing total inductance until $L \sim 0.8\,Z\,t$, where Z is the impedance of the driver and t is the rise time of the current. For our proposed driver and load, that means that the optimum total inductance is ~10 nH. The total inductance of the constant-impedance MITL design above *with a Z51 load* is ~10.6 nH. (Note that the Z51 load is one of the lowest-inductance dynamic loads that would be fielded, and other loads would have a higher initial inductance.) We can therefore increase overall coupling efficiency if we can slightly lower the MITL inductance. We can decrease the inductance (gap) of the feed, but we need to monitor all of the Z_{flow} parameters of the MITL. Do we have a 2D EM PIC code justification for these arbitrary MITL geometry changes? Yes, because the Z_{flow} model has been benchmarked by Ottinger *et al.*[32] against PIC calculations. We believe that designing an MITL, based on the Z_{flow} MITL model, that has "good" Z_{flow}, E/cB, and loss current densities should work well. The use of a z-pinch load forces the MITL to operate in the super-insulated regime with decreasing E/cB and increasing Z_{flow} going radially inward, and these facts alone allow significant MITL design flexibility that might not exist with other loads.

Consider that the outer MITL segments of the 2-Ω MITL have electron-loss current densities nearly 1000 times lower than the "maximum acceptable" electron-loss current density found in the inner MITL segments. We propose a variable-impedance MITL with an outer MITL impedance of 1.5 Ω and an inner MITL impedance of 2 Ω. There are no other changes to the simulation from the constant-impedance MITL case. We address the radial disparity in loss current density by decreasing the gap (decreasing the impedance and increasing the loss current) at the large-radius (outer) entrance to the variable-impedance MITL. The variable-impedance MITL is then composed of a smoothly varying impedance (geometric straight line) to the unchanged inner segment of the variable-impedance MITL. As before, we divide the variable-impedance MITL into ten segments of 0.4010-ns length each. The variable-impedance MITL profile and other information are shown in Table II.

We model the idealized variable-impedance disk MITL that extends from the region near the insulator stack to the constant-gap MITL section at a radius of 30 cm. The initial height of the vacuum feed at a radius of 155 cm is unchanged at 11.43 cm. Figure 1(b) includes the vacuum flare at an angle of

TABLE II. Radius, circumference, gap, impedance, and inductance of the ten MITL segments used in the *SCREAMER* calculations.

MITL segment	Radius centroid (cm)	Circular centroid (cm)	Calculated gap (cm)	Local impedance (Ω)	Local inductance (H) ($\times 10^{-10}$)
1	144.2565	906.4	3.621	1.505	6.0384
2	132.2295	830.8	3.345	1.517	6.0858
3	120.2025	755.3	3.070	1.531	6.1427
4	108.1755	679.7	2.794	1.549	6.2122
5	96.1485	604.1	2.518	1.570	6.2991
6	84.1215	528.6	2.242	1.598	6.4109
7	72.0945	453.0	1.966	1.635	6.5600
8	60.0675	377.4	1.690	1.687	6.7689
9	48.0405	301.8	1.414	1.765	7.0822
10	36.0135	226.3	1.139	1.896	7.6049

~31.7° and shows the electrode profile for the 1.5-Ω to 2-Ω variable-impedance disk MITL. The drawing provides detailed radial location and gap dimensions for the variable-impedance disk MITL. The height of the outer MITL is smaller than in the 2-Ω case. Note that the vertical scale in the figure is four times the horizontal scale for clarity.

We expect that this change in MITL profile will leave the electron losses on the inner MITL segment nearly unchanged while increasing the electron losses in the outer MITL segments. The largest percentage increase in electron losses will be at the outermost segment of the MITL, which has the largest absolute decrease in gap. The change to a variable-impedance (1.5-Ω to 2.0-Ω) MITL results in a lowering of the disk MITL inductances to ~6.52 nH each (from 8.07 nH each for the 2-Ω case). The total geometric inductance of the vacuum feed decreases from 10.56 nH to 9.8 nH. (This inductance is the paralleled inductance of the A- and B-level feeds, the PHC, the disk MITL, and the Z51 load.)

A. *SCREAMER* simulation of a 1.5-Ω to 2.0-Ω variable-impedance MITL

A SCREAMER calculation for the 15-TW driver using 1.5-Ω to 2-Ω variable-impedance MITLs and a z-pinch load gives us detailed voltage, current, and MITL information in time and space. The overall current performance is shown in Fig. 7, where we plot the total current in the load and the current exiting the A- and B-level MITLs. The A- and B-level currents reflect the new increased electron losses to the anode in the variable-impedance MITL early in the pulse. The total current, as before, includes additional losses in the vacuum PHC. We see that the peak current driving the load is ~10.4 MA, an increase from the ~10 MA of the 2-Ω MITL simulation. Note that the implosion occurs at a time of ~253 ns (relative to the start of the simulation). This is 3 ns faster than the implosion time of the constant-impedance case. Increasing the z-pinch mass slightly would give the same implosion time and implosion velocity as the 2-Ω case but with a slightly higher current than the 10.4 MA seen in this variable-impedance MITL calculation. This would provide a more exact A–B comparison of the two MITL configurations.

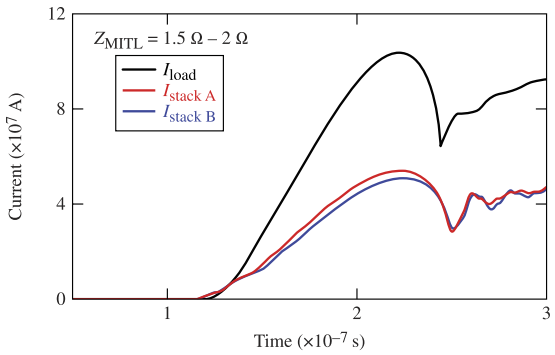

FIG. 7. Calculated total current (black solid curve), A-level current (red solid curve), and B-level current (blue solid curve) as functions of time.

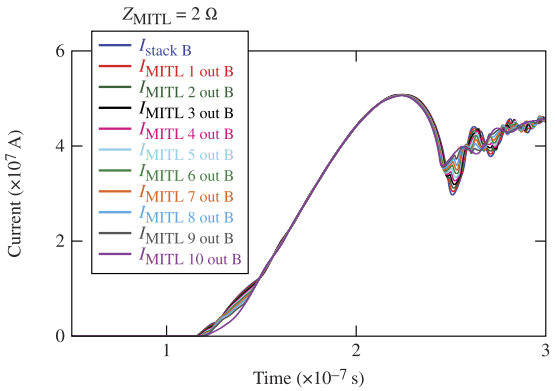

FIG. 8. Calculated currents in each MITL segment as functions of time for the variable-impedance MITL. The differences in the various currents seen at ~120 ns to 150 ns reflect losses during the setup of magnetic insulation.

The B-level MITL current information in Fig. 8 is from ten locations after each MITL segment. The figure clearly shows increased MITL losses early in time. The peak current is higher than the current for the 2-Ω constant-impedance MITL. Once full insulation is achieved (>150 ns), there are no further current losses observed until the time of implosion.

In Fig. 9, we plot the voltages after each segment for the variable-impedance MITL. The voltages of each MITL segment are slightly lower than the 2-Ω case and decrease as the MITL radii decrease because of reduced enclosed inductance. The various parameters of the MITL at the time of peak voltage (175 ns) are shown for reference in Table III. The local electric field at each MITL segment is calculated and also shown in Table III.

Several items of interest are seen in Table III and from a comparison with the results in Table I:

1. With this variable MITL impedance, the flow impedance Z_{flow} increases smoothly with decreasing MITL radius. In all

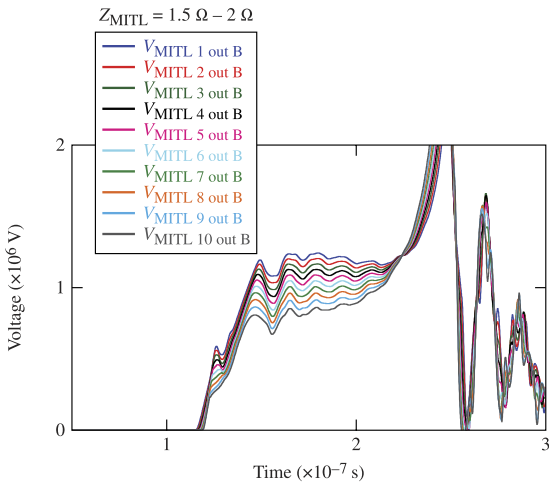

FIG. 9. Calculated voltages of each MITL segment with time. The voltages decrease radially inward.

TABLE III. Listing of B-level MITL parameters from *SCREAMER* calculations for a variable-impedance MITL.

MITL segment	Radial location (cm)	AK gap (cm)	Z_{vac} (Ω)	V_a (MV)	E_c (kV/cm)	I_a (MA)	Z_r (Ω)	Z_{flow} (Ω)	I_c (MA)	I_{vac} (kA)	E/cB	h_{sh} (mm)	h_{sh}/gap
1	144.95	3.639	1.505	1.231	338	2.92	0.422	1.479	2.799	121	0.285	0.62	0.0171
2	132.85	3.361	1.517	1.188	353	2.92	0.407	1.493	2.809	111	0.273	0.54	0.0160
3	120.75	3.083	1.531	1.145	371	2.92	0.392	1.508	2.820	101	0.260	0.47	0.0151
4	108.65	2.806	1.548	1.103	393	2.92	0.378	1.530	2.829	91	0.248	0.40	0.0142
5	96.55	2.528	1.570	1.060	419	2.92	0.363	1.549	2.840	81	0.234	0.33	0.0131
6	84.45	2.250	1.598	1.017	452	2.92	0.348	1.579	2.850	72	0.221	0.27	0.0121
7	72.35	1.973	1.635	0.966	490	2.92	0.331	1.617	2.858	62	0.205	0.22	0.0110
8	60.25	1.695	1.687	0.923	545	2.92	0.316	1.671	2.867	53	0.189	0.17	0.0098
9	48.15	1.417	1.765	0.880	621	2.92	0.301	1.750	2.876	44	0.172	0.12	0.0085
10	36.05	1.140	1.895	0.829	727	2.92	0.284	1.882	2.887	33	0.151	0.08	0.0070

of the segments of the MITL, Z_{flow} is capped by the *local* MITL vacuum impedance.

2. The cathode current increases with decreasing radius (or, equivalently, the vacuum electron flow decreases with decreasing radius). The absolute values of the cathode current are higher than in the 2-Ω MITL case. The magnitude of the vacuum current is higher for MITL segment 1 in the variable-impedance MITL than in the 2-Ω MITL, but by the time MITL segment 10 is reached, the vacuum currents are almost identical. The smaller gap in MITL segment 1 (higher E) is the cause of the increased vacuum current.
3. The running impedance is lower for all MITL segments in the variable-impedance MITL case than for the same segments in the 2-Ω MITL case. The ratio E/cB continues to decrease strongly with decreasing radius. The value of E/cB starts larger because of the smaller gaps (lower impedance and higher electric field) at larger radii, but ends up nearly the same at the inner radii as the 2-Ω results in Table I. Even the larger value of E/cB is quite safe from the standpoint of magnetic insulation.
4. The size of the electron sheath starts larger than in the 2-Ω case, but decreases rapidly with decreasing radius. The sheath size at the inner edge of the MITL is similar to the 2-Ω case shown in Table I.

The SCREAMER calculations show that the variable-impedance MITL continues to be robustly insulated with decreasing radius. The reduction in the vacuum-electron-flow current means that electron retrapping is taking place. The fraction of the current in vacuum flow at peak voltage remains small. While the sheath size and vacuum current are higher in MITL segment 1 than in 2-Ω MITL segment 1, they are nearly the same as those of the 2-Ω MITL in MITL segment 10.

The current losses in each segment of the variable-impedance MITL continue to show that the lowest electron-loss current is on the outer MITL segments (largest gap), with increasing loss current densities on the inner MITL segments (see Figs. 10 and 11). The variable-impedance MITL has increased the absolute level of MITL losses on the outer MITL segments, but still not to the same level as on MITL segment 10. The difference between the outer MITL segment and inner MITL segment loss current density between the 2-Ω case (Fig. 6) and the variable-impedance MITL has been reduced. Even though the total early-time MITL losses are increased, the current driving the load is increased because of the reduced MITL inductance. Figure 10 clearly shows the differences in the turn-on time of the losses and the turn-off time of the losses for each MITL segment. Electron losses *always* start at the MITL segments that have the highest electric fields, and the losses always end when the local magnetic field is large enough to insulate the vacuum line at that MITL segment. The outermost MITL segment (segment 1) is the last to be fully insulated in these calculations.

Examination of the values of the electron-loss current density in each segment of the variable-impedance MITL shows that the lowest electron-loss current density remains in the outer MITL segments (largest gap), with increasing loss current densities in the inner MITL segments (see Fig. 11). The electron-loss current density in the inner MITL segment is 55 times larger than that on the outer MITL segment. Compare these electron-loss current densities with those seen in Fig. 6.

The variable-impedance MITL design shown here (1.5 Ω to 2 Ω) is not intended to be the best or final design. It is only indicative of the improvements that can be made in overall MITL

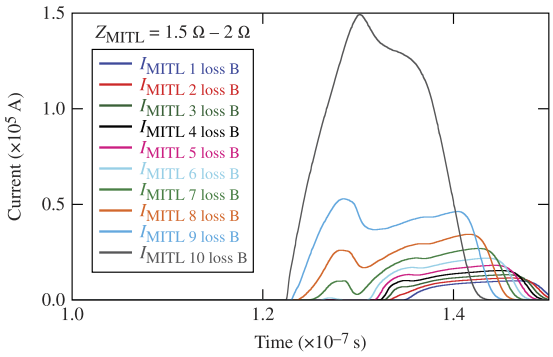

FIG. 10. Electron-loss currents in each MITL segment for the variable-impedance MITL, where the largest current losses occur with inner MITL segment 10. z-pinch stagnation is at ~255 ns.

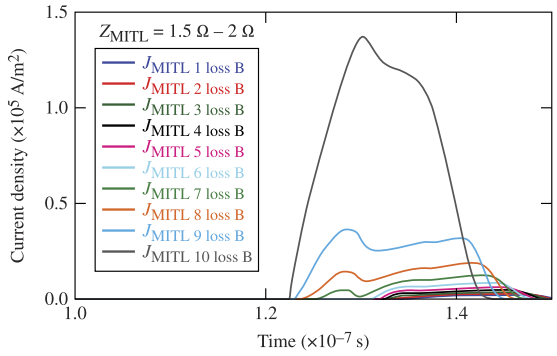

FIG. 11. Electron-loss current density in each MITL segment of the variable-impedance MITL, where the largest current-density losses occur with inner MITL segment 10.

inductance while maintaining robust and safe magnetic insulation. These designs do not address design refinements such as a gradual impedance taper at the radius where the variable-impedance MITL meets the constant-gap MITL, nor do they take into account the transition in the vacuum flare profile to the outer MITL.

We note that Pointon and Savage[9] showed with 2D PIC simulations that electron flow in a disk MITL with a varying impedance is improved when the rate of change of impedance with radius is small. They observed electron vortices (leading to minor losses) when they modeled disk MITLs that did not have a constant impedance. We can partially address this concern by designing a variable-impedance MITL having a constant impedance rate of change with radius (dZ/dr = constant). For the case of a 1.5-Ω to 2-Ω disk transmission line having a constant dZ/dr, the solution for the height of the gap with radius is straightforward: $h = 0.035\,44\,r - 0.000\,069\,32\,r^2$. This is the type of solution that fits within the Z_{flow} framework but addresses potential physics issues seen in more-detailed PIC simulations. The modified gaps herein change the inductance minimally and do not change the Z_{flow} parameters.

VII. DISCUSSION

The electron losses seen at each MITL segment are a strong function of local impedance (gap) and local electric field. The differences in electron-loss current density are driven, first, by the higher electric fields seen on the inner MITL segments and, second, by the differences in the surface areas of the inner MITL segments versus the outer MITL segments. We see that the losses in the inner MITL segment for both MITL cases are much higher than those in the outer MITL segments. This suggests, on the one hand, that further decreases in the impedance at the outer MITL radius will lower total inductance. On the other hand, assembly tolerances of the MITLs, debris on the MITLs, and defects in their surfaces could cause MITL electron-loss current densities in excess of the calculated values. A careful comparison of the reliability risks of lower-inductance MITLs versus the benefits of better coupling to the load needs to be made.

Further decreases in MITL impedances (gaps) at the outer MITL radius could increase MITL losses in the outer MITL segments compared with higher-impedance MITL designs (1.5 Ω and 2 Ω). However, the total inductance gains with decreasing outer MITL impedance will be proportionally smaller owing to the irreducible inductances in other parts of the circuit (the insulator stack, the PHC, the inner disk feed, and the load). Even in our two cases, a reduction in the inductance of each disk MITL by 1.56 nH (from 8.075 nH in the 2-Ω case to 6.52 nH in the 1.5-Ω to 2-Ω case) only reduced the total inductance of the system by 0.76 nH (the final inductance is effectively the inductance reduction of two MITLs in parallel) from 10.56 nH to 9.8 nH. Further gains in total inductance will begin to asymptote with continued reductions in outer MITL impedance. For example, for Z_{outer} = 1.0 Ω (2.51-cm AK gap) and Z_{inner} = 2.0 Ω, the total inductance is lowered to 9.05 nH. It is unfortunate that the cost (and time) invested in building large-diameter MITLs leads to very conservative design decisions and precludes a thorough experimental study of riskier but more efficient MITL designs.

VIII. CONCLUSION

We have shown two different MITL designs, based on the Z_{flow} MITL model, that were developed with the SCREAMER circuit code. The 2-Ω constant-impedance MITL is very similar to the well-tested Z-machine MITLs, and the variable-impedance (1.5-Ω to 2-Ω) MITL is one possible improvement in MITL inductance and overall driver coupling efficiency. Both designs have robust magnetic insulation as suggested by the Z_{flow} model used in SCREAMER. Validation of vacuum power flow with highly resolved PIC codes is always required for actual designs. We have shown that we can design MITLs using SCREAMER for the case of a z-pinch load but suggest that the same design philosophy can be used with arbitrary drivers and loads.

ACKNOWLEDGMENTS

This material is based upon work supported by the Department of Energy National Nuclear Security Administration under Award No. DE-NA0001944, the University of Rochester, and the New York State Energy Research and Development Authority.

This report was prepared as an account of work sponsored by an agency of the U.S. Government. Neither the U.S. Government nor any agency thereof, nor any of their employees, makes any warranty, express or implied, or assumes any legal liability or responsibility for the accuracy, completeness, or usefulness of any information, apparatus, product, or process disclosed, or represents that its use would not infringe privately owned rights. Reference herein to any specific commercial product, process, or service by trade name, trademark, manufacturer, or otherwise does not necessarily constitute or imply its endorsement, recommendation, or favoring by the U.S. Government or any agency thereof. The views and opinions of the authors expressed herein do not necessarily state or reflect those of the U.S. Government or any agency thereof.

REFERENCES

[1]R. B. Spielman, F. Long, T. H. Martin, J. W. Poukey, D. B. Seidel *et al.*, "PBFA II-Z: A 20-MA driver for Z-pinch experiments," in *Tenth IEEE International Pulsed Power Conference*, edited by W. L. Baker and G. Cooperstein (IEEE, New York, 1995), Vol. 1, p. 396, http://ieeexplore.ieee.org/document/596512/.

[2]R. B. Spielman, S. F. Breeze, C. Deeney, M. R. Douglas, F. Long *et al.*, "PBFA Z: A 20-MA Z-pinch driver for plasma radiation sources," in *Proceedings of the 11th International Conference on High Power Particle Beams*, edited by K. Jungwirth and J. Ullschmied (Institute of Plasma Physics, Czech Academy of Sciences, Prague, Czech Republic, 1996), Vol. I, p. 150, http://www.iaea.org/inis/collection/NCLCollectionStore/_Public/28/055/28055908.pdf?r=1.

[3]R. B. Spielman, C. Deeney, G. A. Chandler, M. R. Douglas, D. L. Fehl *et al.*, "Z: A precision 200-TW, 2-MJ Z-pinch x-ray source," Bull. Am. Phys. Soc. **42**, 1947 (1997), http://flux.aps.org/meetings/YR97/BAPSDPP97/abs/S4000002.html.

[4]R. B. Spielman, W. A. Stygar, K. W. Struve, and J. F. Seamen, "PBFA Z: A 55 TW/4.5 MJ electrical generator," in *Proceedings of the 1997 Particle Accelerator Conference*, edited by M. Comyn, M. K. Craddock, M. Reiser, and J. J. Thomson (IEEE, Piscataway, NJ, 1997), Vol. 1, p. 1235, http://ieeexplore.ieee.org/document/749986/.

[5]D. D. Bloomquist, R. W. Stinnett, D. H. McDaniel, J. R. Lee, A. W. Sharpe *et al.*, "Saturn, a large area x-ray simulation accelerator," in *6th IEEE Pulsed Power Conference*, edited by B. H. Bernstein and P. J. Turchi (IEEE, New York, 1987), p. 310, https://www.researchgate.net/publication/236355229_Saturn_A_large_area_x-ray_simulation_accelerator.

[6]R. B. Spielman, R. J. Dukart, D. L. Hanson, B. A. Hammel, W. W. Hsing *et al.*, "Z-pinch experiments on Saturn at 30 TW," AIP Conf. Proc. **195**, 3 (1989).

[7]D. B. Seidel, M. L. Kiefer, R. S. Coats, T. D. Pointon, J. P. Quintenz *et al.*, "The 3-D, electromagnetic, particle-in-cell code, QUICKSILVER," Int. J. Mod. Phys. C **02**, 475 (1991).

[8]T. D. Pointon, W. A. Stygar, R. B. Spielman, H. C. Ives, and K. W. Struve, "Particle-in-cell simulations of electron flow in the post-hole convolute of the Z accelerator," Phys. Plasmas **8**, 4534 (2001).

[9]T. D. Pointon and M. E. Savage, "2-D PIC simulations of electron flow in the magnetically insulated transmission lines of Z and ZR," in *2005 IEEE Pulsed Power Conference* (IEEE, Piscataway, NJ, 2005), p. 151.

[10]T. D. Pointon, W. L. Langston, and M. E. Savage, "Computer simulations of the magnetically insulated transmission lines and post-hole convolute of ZR," in *2007 16th IEEE International Pulsed Power Conference* (IEEE, Piscataway, NJ, 2007), Vol. 1, p. 165.

[11]J. M. Creedon, "Relativistic Brillouin flow in the high ν/γ diode," J. Appl. Phys. **46**, 2946 (1975).

[12]J. M. Creedon, "Magnetic cutoff in high-current diodes," J. Appl. Phys. **48**, 1070 (1977).

[13]C. W. Mendel, Jr., "Planar one-dimensional magnetically insulated electron flow for arbitrary canonical-momentum distribution," J. Appl. Phys. **50**, 3830 (1979).

[14]C. W. Mendel, Jr., J. P. VanDevender, and G. W. Kuswa, "Determination of line voltage in self-magnetically insulated flows," in *2nd IEEE International Pulsed Power Conference*, edited by A. H. Guenther and M. Kristiansen (IEEE, Piscataway, NJ, 1979), p. 153, http://www.iaea.org/inis/collection/NCLCollectionStore/_Public/16/076/16076157.pdf.

[15]J. P. VanDevender, "Self-magnetically insulated power flow," in *2nd IEEE International Pulsed Power Conference*, edited by A. H. Guenther and M. Kristiansen (IEEE, Piscataway, NJ, 1979), p. 55, http://www.iaea.org/inis/collection/NCLCollectionStore/_Public/16/076/16076157.pdf.

[16]J. P. VanDevender, "Long self-magnetically insulated power transport experiments," J. Appl. Phys. **50**, 3928 (1979).

[17]J. P. VanDevender, J. T. Crow, B. G. Epstein, D. H. McDaniel, C. W. Mendel *et al.*, "Self-magnetically insulated electron flow in vacuum transmission lines," Physica B+C **104**, 167 (1981).

[18]C. W. Mendel, D. B. Seidel, and S. E. Rosenthal, "A simple theory of magnetic insulation from basic physical considerations," Laser Part. Beams **1**, 311 (1983).

[19]C. W. Mendel, Jr., D. B. Seidel, and S. A. Slutz, "A general theory of magnetically insulated electron flow," Phys. Fluids **26**, 3628 (1983); Erratum, **27**, 1563(E) (1984).

[20]M. S. Di Capua, "Magnetic insulation," IEEE Trans. Plasma Sci. **11**, 205 (1983).

[21]P. A. Miller and C. W. Mendel, Jr., "Analytic model of applied-B ion diode impedance behavior," J. Appl. Phys. **61**, 529 (1987).

[22]S. E. Rosenthal, "Characterization of electron flow in negative- and positive-polarity linear-induction accelerators," IEEE Trans. Plasma Sci. **19**, 822 (1991).

[23]C. W. Mendel, S. E. Rosenthal, and D. B. Seidel, "Low-pressure relativistic electron flow," Phys. Rev. A **45**, 5854 (1992).

[24]C. W. Mendel, Jr., M. E. Savage, D. M. Zagar, W. W. Simpson, T. W. Grasser *et al.*, "Experiments on a current-toggled plasma-opening switch," J. Appl. Phys. **71**, 3731 (1992).

[25]C. W. Mendel, Jr., "Status of magnetically-insulated power transmission theory," SAND-95-3014C, Sandia National Laboratories, Albuquerque, NM, 1995, https://www.osti.gov/servlets/purl/238537.

[26]C. W. Mendel, Jr. and S. E. Rosenthal, "Modeling magnetically insulated devices using flow impedance," Phys. Plasma **2**, 1332 (1995).

[27]C. W. Mendel, Jr. and S. E. Rosenthal, "Dynamic modeling of magnetically insulated transmission line systems," Phys. Plasma **3**, 4207 (1996).

[28]C. W. Mendel, Jr. and D. B. Seidel, "Flow impedance in a uniform magnetically insulated transmission line," Phys. Plasma **6**, 4791 (1999).

[29]P. F. Ottinger and J. W. Schumer, "Rescaling of equilibrium magnetically insulated flow theory based on results from particle-in-cell simulations," Phys. Plasma **13**, 063109 (2006).

[30]W. A. Stygar, T. C. Wagoner, H. C. Ives, P. A. Corcoran, M. E. Cuneo *et al.*, "Analytic model of a magnetically insulated transmission line with collisional flow electrons," Phys. Rev. Spec. Top.–Accel. Beams **9**, 090401 (2006).

[31]P. F. Ottinger, J. W. Schumer, D. D. Hinshelwood, and R. J. Allen, "Generalized model for magnetically insulated transmission line flow," IEEE Trans. Plasma Sci. **36**, 2708 (2008).

[32]P. F. Ottinger, J. W. Schumer, D. D. Hinshelwood, R. J. Allen, Benchingmark and implementation of a generalized MITL flow model, in *17th IEEE International Pulsed Power Conference*, edited by R. D. Curry (IEEE, Piscataway, NJ, 2009), p. 1176.

[33]M. L. Kiefer and M. M. Widner, "SCREAMER—A single-line pulsed-power design tool," in *Fifth IEEE Pulsed Power Conference (PPC)*, edited by P. J. Turchi and M. F. Rose (IEEE, Piscataway, NJ, 1985), p. 685, https://inis.iaea.org/search/search.aspx?orig_q=RN:18080265.

[34]R. B. Spielman and Y. Gryazin, "SCREAMER v4.0—A powerful circuit analysis code," in *2015 IEEE Pulsed Power Conference (PPC)* (IEEE, Piscataway, NJ, 2015).

[35]W. A. Stygar, P. A. Corcoran, H. C. Ives, R. B. Spielman, J. W. Douglas *et al.*, "55-TW magnetically insulated transmission-line system: Design, simulations, and performance," Phys. Rev. Spec. Top.–Accel. Beams **12**, 120401 (2009).

[36]M. Savage, J. Martin, T. Pointon, C. Mendel, D. Jackson *et al.*, "Precision electron flow measurements in a disk transmission line," Sandia National Laboratories, Albuquerque, NM, Report SAND2007-8156, 2008, https://prod.sandia.gov/techlib-noauth/access-control.cgi/2007/078156.pdf.

[37]J. P. VanDevender, T. D. Pointon, D. B. Seidel, K. W. Struve, C. Jennings *et al.*, "Requirements for self-magnetically insulated transmission lines," Phys. Rev. Spec. Top.–Accel. Beams **18**, 030401 (2015).

[38]R. B. Spielman, D. H. Froula, G. Brent, E. M. Campbell, D. B. Reisman *et al.*, "Conceptual design of a 15-TW pulsed-power accelerator for high-energy-density–physics experiments," Matter Radiat. Extremes **2**, 204 (2017).

[39]T. W. L. Sanford, J. A. Halbleib, J. W. Poukey, A. L. Pregenzer, R. C. Pate *et al.*, "Measurement of electron energy deposition necessary to form an anode plasma in Ta, Ti, and C for coaxial Bremsstrahlung diodes," J. Appl. Phys. **66**, 10 (1989).

[40]B. C. Franke, R. P. Kensek, and T. W. Laub, "ITS version 5.0: The integrated TIGER series of coupled electron/photon Monte Carlo transport codes with CAD geometry," Sandia National Laboratories, Report No. SAND–2004-5172, 2005, https://www.osti.gov/servlets/purl/877725-5A1CKs/.